ISSN 0016-8521, Geotectonics, 2015, Vol. 49, No. 5, pp. 439–450. © Pleiades Publishing, Inc., 2015.

Application of Kinematic Vorticity Techniques for Mylonitized Rocks in Al Amar Suture, Eastern Arabian Shield, Saudi Arabia[1]

Z. Hamimi[a], O. M. K. Kassem[b,c] and M. N. El-Sabrouty[c]

[a]Geology Department, Faculty of Science, Banha University, Banha 13518, Egypt

[b]SGSRC, Department of Geology, Faculty of Science, King Saud University, P.O. Box 2455, Riyadh 11451, Saudi Arabia

[c]Geology Department, National Research Center, Al-Behoos Str., 12622 Dokki, Cairo, Egypt

e-mail: yahiahamimi@gmail.com

Received October 13, 2014

Abstract—The rotation of rigid objects within a flowing viscous medium is a function of several factors including the degree of non-coaxiality. The relationship between the orientation of such objects and their aspect ratio can be used in vorticity analyses in a variety of geological settings. Method for estimation of vorticity analysis to quantitative of kinematic vorticity number (W_m) has been applied using rotated rigid objects, such as quartz and feldspar objects. The kinematic vorticity number determined for high temperature mylonitic Abt schist in Al Amar area, extreme eastern Arabian Shield, ranges from ~0.8 to 0.9. Obtained results from vorticity and strain analyses indicate that deformation in the area deviated from simple shear. It is concluded that nappe stacking occurred early during an earlier thrusting event, probably by brittle imbrications. Ductile strain was superimposed on the nappe structure at high-pressure as revealed by a penetrative subhorizontal foliation that is developed subparallel to tectonic contacts versus the underlying and overlying nappes. Accumulation of ductile strain during underplating was not by simple shear but involved a component of vertical shortening, which caused the subhorizontal foliation in the Al Amar area. In most cases, this foliation was formed concurrently with thrust sheets imbrications, indicating that nappe stacking was associated with vertical shortening.

Keywords: kinematic analysis, pure shear, simple shear, Al Amar area, Eastern Arabian Shield

DOI: 10.1134/S0016852115050040

INTRODUCTION

The Neoproterozoic basement rocks outcropping in both sides of the Red Sea form the Arabian-Nubian Shield (ANS). The ANS extends over 3500 km north-south (maximum width ~1500 km), and is traditionally subdivided into Arabian Shield (AS) located to the east of the Red Sea and Nubian Shield (NS) occupying the western flank [66]. It is regarded as a world-class laboratory for the study of Neoproterozoic crustal processes [25]. R. J. Stern and P. R. Yohnson [59] believed that the ANS constitutes one of the largest best exposed tracts of juvenile Precambrian continental crust on the Earth and its history is intimately linked with a Neoproterozoic Supercontinent cycle. The concept of the supercontinent cycle has emerged by [64–66] as a simplistic initiative, and evolved in the past two decades to more complicated ideas proved by zircon geochronology, isotope geochemistry, mantle tomography, and ever-more sophisticated numerical and dynamic modeling [42]. Interactions of the supercontinent cycle and the history of the Earth's geosphere, atmosphere, hydrosphere, cryosphere and biosphere have been documented. With respect to the ANS, the cycle began with fragmentation, rifting and dispersal of Rodina in the early Cryogenian [40], continued with the opening and closing of one or two oceanic basins [7, 58], and ended with the convergence of fragments of East and West Gondwana lands and the formation of Greater Gondwana [58] or Pannotia [12]. The ANS is subdivided into a college of tectonic terranes separated by ophiolite-decorated sutures, high strain transpressional shear zones and post-accretionary fault zones. Older AS terranes include Jiddah (870–740 Ma; [35]) and Asir (850–750 Ma; [27]), intermediate terranes include Midayan (780–710 Ma; [1, 2, 21]), and younger terranes include Ar Rayan (>670; [55]) and Ad Dawadimi (674 ± 6 Ma; [11]).

Many authors have tried to understand the kinematics, deformation conditions, and tectonic significance of brittle-ductile shear zones [17–20]. General techniques have been developed to quantitatively evaluate both strain and vorticity in deformed rocks [29, 31, 45, 48, 54, 55, 61]. However, a lot of studies have quantified the strain and vorticity path in naturally deformed rocks [56, 62]. In the study of deformation in ductile shear zones, it is commonly assumed that strain has accumulated by progressive simple shear [45, 55]. Nevertheless, other types of steady-state pro-

[1] The article is published in the original.

gressive deformation are also possible. For deformation with no volume change, three types of plane-strain steady deformation can be defined: pure shear, simple shear and general non-coaxial shear that is intermediate between the other two [3, 16, 28, 34, 45, 48, 54]. For these types of deformation, the differences in the type of associated flow can be described in terms of the degree of non-coaxiality [19, 37–39, 44]. The degree of non-coaxiality of deformation gives a measure of the relative contribution of rotation to stretching during deformation. In the analysis of finite deformation, the degree of non-coaxiality is commonly expressed by the mean kinematic vorticity number; W_m [45]. The degree of non-coaxiality of deformation presents a measure of the relative contribution of rotation to stretching during deformation. Additionally, the Rigid Grain Net (RGN) is used to unify the most commonly used Wm plots by comparing the distribution of theoretical and natural tailless porphyroclasts within a flowing matrix.

The present study investigates the effect of different combinations of pure and simple shears, matrix rheology, object aspect ratio and resultant flow perturbation on the development of shape-preferred orientation of a population of rigid objects during progressive deformation for the Abt Schist, metasedimentry rocks and mylonitized granite in the Al Amar area. The study aims to elucidate the orogenic stages during nappe formation, and to detect the orientation of rigid objects during progressive deformation.

GEOLOGICAL SETTING

The Neoproterozoic basement rocks exposed in the area (Fig. 1) are discriminated into three main lithologies; Abt Schist Formation, Al Amar Group and intrusive rocks. The Abt Formation is outcropping as a thick immature sedimentary unit exhibiting low grade greenschist facies metamorphism and westward facing (younging) direction. It is foliated, folded and lineated, and occasionally encompasses small marble bands. Foliation strikes N-S and dipping towards the W-direction in moderate to steep angles. It is related to an older D_1 deformation phase. During a subsequent D_2 phase, tight and intrafolial folds with N-S axial planes are formed. Under the microscope, the Abt Formation is discriminated into muscovite-biotite-quartz-feldspar schist, and feldspathic and volcanic metagreywackes.

The Abt Schist Formation occupies enormous province in Ad Dawadimi terrane which is covered also by syenogranite, alkali-feldspar granite, layered gabbro, and ophiolite mélange zones with forearc affinity. The juxtaposition of the immature sediments with forearc units led [11] to conclude that Ad Dawadimi terrane has many similarities with more modern accretionary environments such as the Franciscan Formation of the western United States [5, 6].

Al Amar Group forms one of the major lithologies exposed at Ar Rayn terrane. It consists of continental-margin volcanic arc comprising intermediate to silicic westward dipping volcanosedimentary sequence and related volcaniclastics. Because of the effect of tectonism and magmatism in the entire Ar Rayn terrane, Amar Group is discriminated into seven N-oriented elongated belts. These belts are intruded by syn- to post-tectonic intrusives (667–580 Ma) including gabbros and extremely sheared granitoids (granite, granodiorite, tonalite and trondhjemite). Andesitic and rhyolitic flows, paragneisses and limestone close to the contact between the volcanosedimentary sequence and the intrusive rocks, especially granitoids.

The mapped area (Fig. 1) lies along the contact between Ad Dawadimi and Ar Rayn terranes which are believed to be the youngest terranes in the ANS at all. Both Ad Dawadimi and Ar Rayn terranes are in direct contact along Al Amar Fault Zone which is known in previous literature as Al Amar-Idsas Fault Zone. Al Amar Fault is a westward steeply dipping N-trending shear zone extending over ≈200 km long, with 0.5–4 km average width [33]. Because of the presence of relatively small-sized lensoidal blocks and fragments of ophiolites and carbonate-altered ultramafic rock (listwaenite and fuchsite-talc schist), this structure is considered by [4], and [7] as a suture zone; namely Al Amar Suture Zone. Of important to denote here that the ophiolitic components are not recognized in the mapped area. Elongated marble outcrops with discrete mineralized quartz veins (pyrite, calcite, fluorite and copper mineralizations) can be seen together along the suture zone [14]. The timing of suturing, trajectory of convergence and sense of shear along Al Amar Suture Zone are debatable. P. Yohnson et al. [24] pointed out the unknown sense of convergence and suggested a dextral horizontal slip based on the S-C shear fabrics that are restrictedly observed in few outcrops. They proposed 620 Ma and 616 Ma as ages of deformation-metamorphism and uplifting, respectively, for both Abt Formation and Al Amar Group depending upon the 607–565 Ma emplacement age for post-tectonic granites that intrude both Ad Dawadimi and Ar Rayn terranes. Within the frame of these previously mentioned ages, Yohnson et al. [26] inferred a suturing age of 620–605 Ma and considered Al Amar Fault as the youngest suture in the ANS, largely simultaneously with the Keraf Suture in the Nubian Shield, and also contemporary with the youngest shearing on the Najd Fault System.

METHODOLOGY

A measure of the orientation and aspect ratios of rigid porphyroclasts rotating in a homogeneously deforming ductile matrix can provide an estimate of both strain path and kinematic vorticity number (W_m) [45, 55, 68]. The basis for this method is the theoretical work of [15, 16, 25, 45] which describes the motion of rigid ellipsoidal particles in a steady non-coaxial flow field. Rigid porphyroclast systems displaying asymmetric recrystallized tails in mylonites are extremely useful

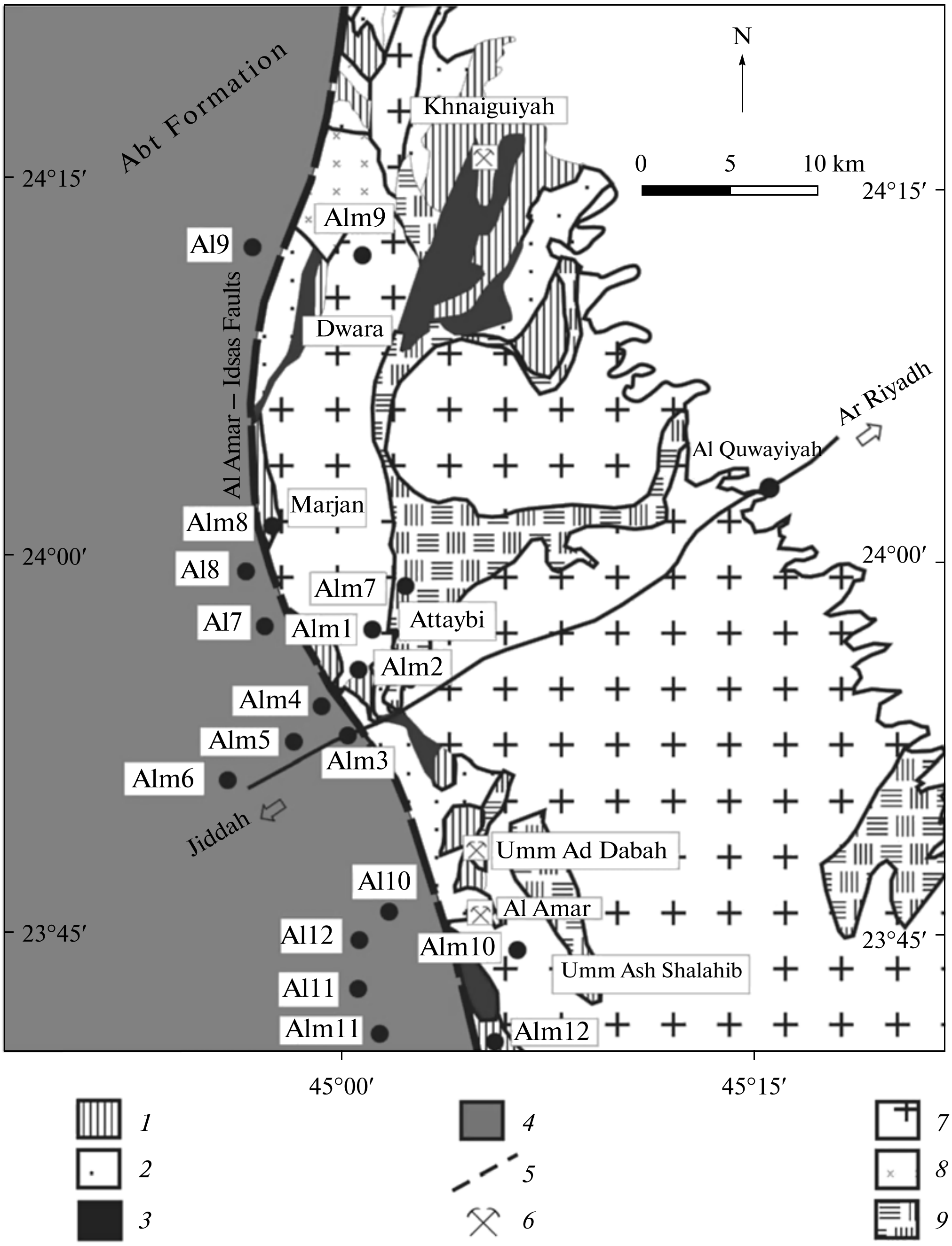

Fig. 1. Geological sketch map of Al Amar area showing sample locations, modified after [12]. *1*—Felsic volcanic rocks; *2*—mafic volcanic rocks; *3*—carbonates and cinerite; *4*—Abt Shist Formation; *5*—fault; *6*—ancient working; *7*—granite, granodiorite, trondhjemite; *8*—mafic intrusive rocks; *9*—undifferentiated metamorphosed volcanic rocks.

for determining shear sense [57] and are also indicators of incremental strains, ductile flow, and finite strain. Using these systems in kinematic vorticity studies depends on the recognition of microstructures that reveal the rotation history of the clasts. The correct identification of clasts that have rotated forward versus those that have rotated backward and those in their stable end orientations is critical for determining the orientation of the eigenvectors of flow. A wide range of clast shapes and orientations are needed. The eigenvector that is inclined relative to the flow plane separates fields of back-rotating versus forward-rotating grains [55]. Backward-rotated objects are generally possible in homogeneous flow regimes only if there is a significant deviation from simple shear and the rotating objects are rigid and more elongate than some critical value [55, 62].

Methods for estimation of kinematic vorticity number (W_m) have been made using rotated rigid

Finite strain data and mean kinematic vorticity number for samples from in the Al Amar region

Sample	Rock type	R_c	W_m (mean values)	R_{xy}	R_{yz}	R_{xz}	S_x	S_y	S_z	K
ALM1	Granodiorite	–	–	1.05	1.07	1.12	1.05	1.01	0.94	0.67
ALM2	Granodiorite	–	–	1.13	1.23	1.39	1.16	1.03	0.84	0.57
ALM3	Abt Schist	5.44	0.97	1.33	2.49	3.3	1.64	1.23	0.50	0.22
ALM4	Abt Schist	6.04	0.97	1.35	2.58	3.49	1.68	1.24	0.48	0.22
ALM5	Abt Schist	3.3	0.91	1.40	3.56	4.99	1.91	1.36	0.38	0.16
ALM6	Abt Schist	3.7	0.93	1.89	2.19	4.13	1.98	1.05	0.48	0.74
ALM7	Metavolcano-sedimentary	–	–	2.18	1.82	3.96	2.05	0.94	0.52	1.43
ALM8	Metavolcano-sedimentary	–	–	2.42	1.71	4.14	2.16	0.89	0.52	2.00
ALM9	Mylonitized granite	–	–	1.16	1.03	1.19	1.11	0.96	0.93	5.18
ALM10	Mylonitized granite	–	–	1.21	1.23	1.49	1.22	1.01	0.82	0.92
ALM11	Abt Schist	4.7	0.95	1.47	2.25	3.31	1.09	1.15	0.51	0.38
ALM12	Metavolcano-sedimentary	–	–	1.34	2.38	3.19	1.62	1.21	0.51	0.25
AL 7	Abt Schist	3.00	0.89	1.40	1.79	2.50	1.52	1.09	0.61	0.50
AL 8	Abt Schist	3.51	0.92	1.41	1.53	2.15	1.45	1.03	0.67	0.76
AL 9	Abt Schist	3.9	0.93	1.75	1.98	3.47	1.83	1.04	0.53	0.77
AL 10	Abt Schist	4.5	0.95	1.33	1.74	2.32	1.46	1.09	0.63	0.45
AL 11	Abt Schist	4.9	0.96	1.61	2.56	4.13	1.88	1.17	0.46	0.39
AL 12	Abt Schist	4.00	0.93	1.85	2.03	3.75	1.91	1.03	0.51	0.82

objects [10, 45–51], deformed vein sets [46, 62], the stretch and rotation of material lines [48] and curved fibres around quartz and feldspar objects [52, 53]. For quantifying the degree of non-coaxiality from rotated rigid objects, the equations governing the rotation of rigid objects in a flowing viscous medium were used [16, 23, 45]. As shown by [16], the sense and rate of rotation of a particle depend on its orientation, axial ratio (R) and the ratio between the elongation in the shear plane and shear strain. For $W_m = 1$, i.e. simple shear, all particles which behave as active markers with $R \geq 1$ will rotate freely as the shear strain increases and the rate of rotation equals the rate of stretching. If W_m is lower than 1, i.e. a component of pure shear accompanies shearing (general or sub-simple shear of [55] and the rotation of particles with progressively smaller aspect ratios is subdued [10]. For any flow regime with $W_m < 1$, not all rigid particles are free to rotate continuously. Particles with an aspect ratio above a certain critical value, R_c, will rotate until they reach a stable orientation. For aspect ratios less than the critical value, rotation is unrestricted. The value of R_c that divides freely rotating objects from those that have reached a stable orientation is a function of the degree of non-coaxiality:

$$W_m = (R_c^2 - 1)/(R_c^2 + 1) \ [40].$$

For successful flow-path analysis, we used the following requirements [40]: (1) largely homogeneous deformation at the sample scale, (2) the grain size of the matrix should be significantly smaller than the grain size of the porphyroclasts, (3) finite strain should be high, (4) object shape should be regular and close to orthorhombic symmetry, and (5) the sample should contain a large number of the spatially well-dispersed objects.

O. M. K. Kassem and Z. Hamimi [30] quantified the finite strain for different deformed rocks in the Al Amar area. Eighteen oriented samples were collected (Fig. 1 and table). The samples include 11 Abt Schist samples, 2 granodiorite samples, 3 metavolcano-sedimentary samples and 2 metagranite samples. The R_f/ϕ method was applied on the quartz and feldspar porphyroclasts and mafic grains to determine the strain recorded in the gneisses [49, 50]. The deformation behavior of plagioclase and K-feldspar is rather similar and therefore feldspar grains are treated together. In other case, the deformation behavior of mica minerals deformed only by slip and amphiboles deformed by twinning and slip on [47]. Felsic minerals are more rigid than some mafic minerals. Therefore, we measure felsic minerals separately from mafic minerals to show the difference between felsic and mafic minerals to the R_f/ϕ analysis.

MICROSTRUCTURE INVESTIGATION

All samples used were collected from Abt Schist Formation, metavolcano-sedimentary and metagranite rocks that exhibit well defined planar and linear fabric elements. Microstructural investigations were made on thin sections cut parallel to the foliation (XY), normal to the foliation and parallel to the lineation (XZ) and normal to the foliation and lineation (YZ). Microstructures and thermobarometric data indicate that feldspar ductility occurs only during high-pressure metamorphism at temperatures ≥450°C, along a major thrust plane [7, 8]. The shear zone extends along Al Amar Fault Zone, which is a N-trending shear zone, steeply dipping westward. The Abt schist exposed in the eastern part of Al Amar Fault Zone and acquires mainly North-South trend with moderately to highly dipping vertical foliations as a result of moderately to highly deformed and well oriented clasts of metsediments (Fig. 2a,b) and fragments of mélange of metavolcanic rocks (Fig. 2c,d). The deformation of the Abt Schist rocks increases towards the shear zone in Al Amar Fault Zone. Deformed samples have elongated felsic and mafic minerals. Felsic minerals are represented by quartz and feldspars, whereas mafic mineral are classified as hornblende, biotite and muscovite (Fig. 2a,b). In some samples, mineral lineations plunge towards the northwest direction. Figure 2a-c shows the quartz—K-feldspar schist. This rock occasionally exhibits rotated felsic rock fragments enclosed in the foliated matrix which consists of elongated hornblende and chlorite.

The volcano-sedimentary sequence encountered in the western part of Al Amar Fault Zone and comprises of weakly to moderately deformed mineral constituents. The weakly deformed volcanic rocks (dacite) contains sanidine, oligoclase and hornblende phenocrysts embedded in crystalline groundmass composed of the same composition associating some quartz crystals (Fig. 2c). The moderatly deformed volcanic rocks (rhyolite) is composed of quartz, K-feldspars (mainly sanidine), and rarely plagioclase phenocrysts enclosed in foliated groundmass of the same composition associating muscovite and biotite (Fig. 2d).

The metagranite is moderately to highly foliated, with a well-developed granoblastic-polygonal texture (Fig. 2e, f). In some places, it displays a weak deformation (Fig. 2g, h) increasing towards Al Amar Fault Zone. Figure 2e, f show elongated feldspars with biotite and hornblende. The highly deformed quartz-rich samples, and the elongated hornblende and chlorite are clearly observed in Fig. 2f. Some granitic rocks are medium to coarse grained and weakly foliated (Fig. 2g, h).

The Abt Schist Formation, metavolcanico-sedimentary and metagranite rocks are composed of different mechanical phases: feldspar, quartz, hornblende and mica. In most situations, feldspar and quartz are the strongest phase while mica is the weakest. Thus strain estimates based on the shapes of feldspar, quartz and mafic grains are suitable for finite strain ellipsoids and the matrix approximates whole rock strain at the scale of thin section or handspecimen. The studied samples reveal that there is no significant difference in deformation behavior between the quartz-mica matrix, the feldspar porphyroclasts and amphibole grains during the accumulation of finite strain at peak metamorphic conditions. Furthermore, finite strain in all types of rocks is of the same order of magnitude. The main-phase foliation is similar in Abt Schist Formation and metavolcanosedimentary rocks, suggesting similar metamorphic behavior in both lithologies.

STRAIN MEASUREMENTS

The field orientations and sample locations for finite strain analysis for Abt schist, metavolcano-sedimentary and deformed granite rocks in the Al Amar area are shown in Fig. 1. The obtained strain data indicate that the long axes of the finite strain ellipsoid (Maximum Extension Direction X axes) in mylonitic rocks in the Al Amar area plunges gently to moderately towards WNW-ESE (Fig. 3). In particular, the mean value for the long axes in all investigated samples displays WNW-ESE trend with a plunge of about 45° (table). The intermediate Y axes trend ENE-WSW with moderate angle of plunges (Fig. 3). In these rocks, the maximum shortening direction (Z) axes steeply plunges towards NNW-SSE (Fig. 3). Thus, the mean finite shortening axes are subvertical and associated with a subhorizontal foliation [33].

The Abt Schist Formation, sheared granitoids and metavolcano-sedimentary rocks are composed of four mechanically different phases: feldspar, quartz, hornblende and mica. The deformation behavior of plagioclase and K-feldspar is rather similar. On the other hand, the deformation behavior of micas differs from those of the felsic grains. Otherwise, quartz is the strongest phase. The studied samples show that there was no significant difference in deformation behavior between the quartz-mica matrix, the feldspar porphyroclasts and amphibole grains during the accumulation of finite strain at peak metamorphic conditions. Furthermore, finite strain in the all types of rocks is of the same order of magnitude. The main-phase foliation is similar in different type of samples, suggesting similar deformation behavior in all rocks types.

The strain data are summarized in table which shows the relative shapes of the strain ellipsoids, i.e. prolate vs oblate. Information on volume strain is needed to infer strain type, i.e. constrictional vs flattening. The strain ellipsoids have oblate strain symmetry. The axial ratios in XZ sections range from 1.70 to 4.80, with S_X ranging from 1.21 to 1.95 for R_f/ϕ method (table) [33] indicated that the axial ratios in XZ sections range from 1.20 to 4.50 and S_X ranging from 1.09 to 1.93 for the Fry method. The stretches in the Z direction, S_Z, range from 0.41 to 0.73, indicating vertical shortening of 27 to 59%. The SY ranges from 0.93 to 1.26 for the R_f/ϕ method, and from 0.93 to 1.26 for the Fry method, showing contraction and extension in this direction. The strain data show the same order of deformation in all rock type, as consistent with qualitative observations in the field and in thin section. With increasing stretch in the X direction and decreasing S_Y, the strain symmetry [22] becomes more

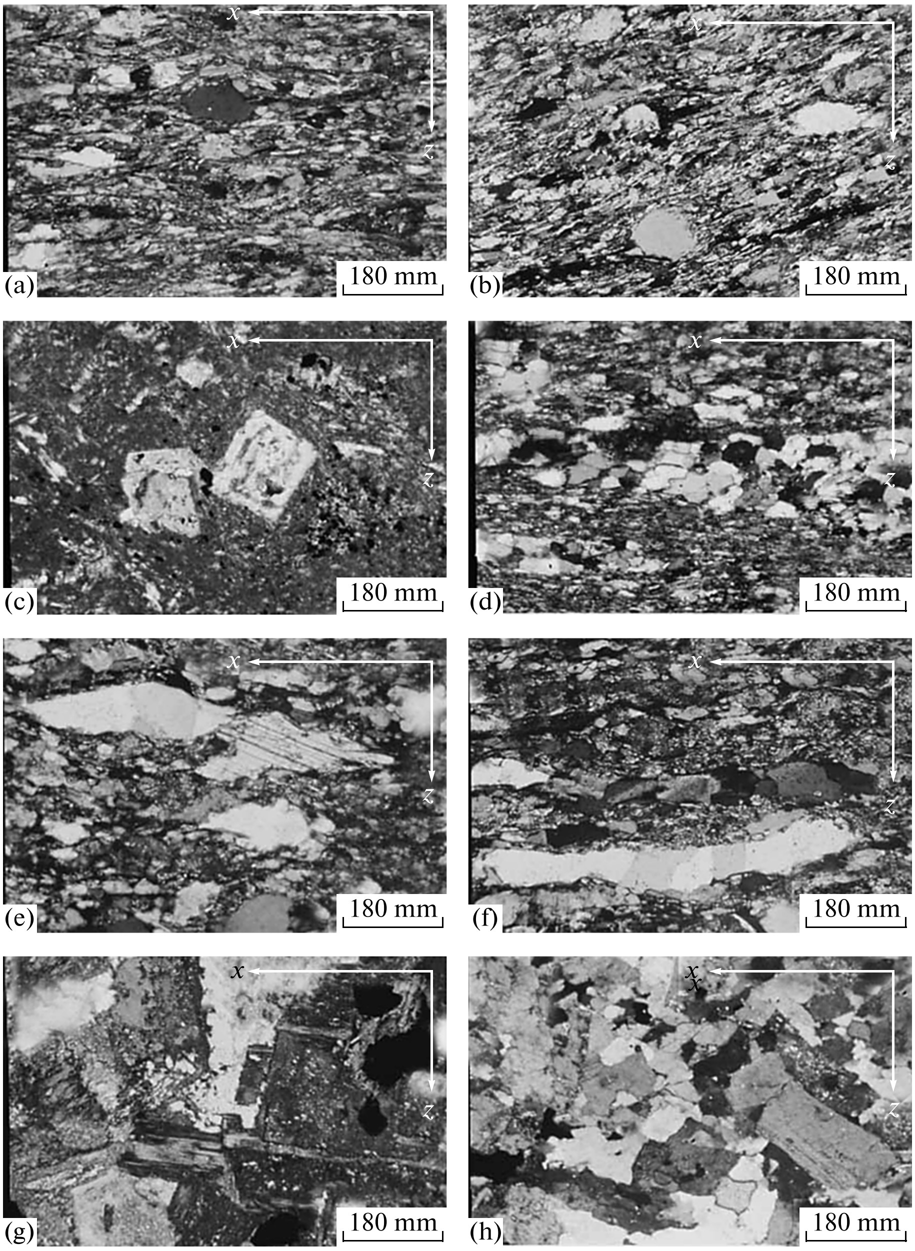

Fig. 2. Microphotographs showing kinematic indicators along Al Amar Suture Zone. a—Highly deformed Abt Schist rocks composed of quartz, K-feldspars, plagioclase and biotite (Sample AL7); b—Well oriented clasts hornblende and biotite grains for Abt Schist rocks associated with rotated quartz grain (Sample AL8); c—Deformed metavolcanic rocks associated with porphyroclasts grains (Sample ALM5); d—Meta-andesite shows porphyritic K-feldspars and plagioclase phenocrysts embedded in a fine grained matrix (Sample ALM6); e—Moderately deformed biotite quartz diorite rocks composed of elongated grains of quartz, K-feldspars, plagioclase and biotite (Sample ALM9); f—Moderately to highly deformed metagranite rocks consisting of quartz, plagioclase and feldspars, with some mafic minerals such as hornblende and biotite (Sample ALM9); g—Weakly foliated samples contain quartz, hornblende, biotite and chlorite in granodiorite rocks (Sample ALM 1); h—Weakly deformed samples containing quartz, feldspars and mafic minerals in granodiorite rocks (Sample ALM2).

prolate (Fig. 4a, b). S_Z shows no obvious correlation between vertical shortening and K (Fig. 4c). Because deviatoric strain depends on all three principal stretches, the positive and negative correlation of S_X and S_Y with the K value does not affect in a correlation between strain magnitude (E_t) and K on the maps [33].

FLOW PATH ANALYSIS

O. M. K. Kassem [32] pointed out that finite-strain data from the same lithology in conjunction with the chemical data (XRF analysis) indicate flattening strain type, suggesting that deformation deviated from simple shear. To quantify the degree of non-coaxiality, a

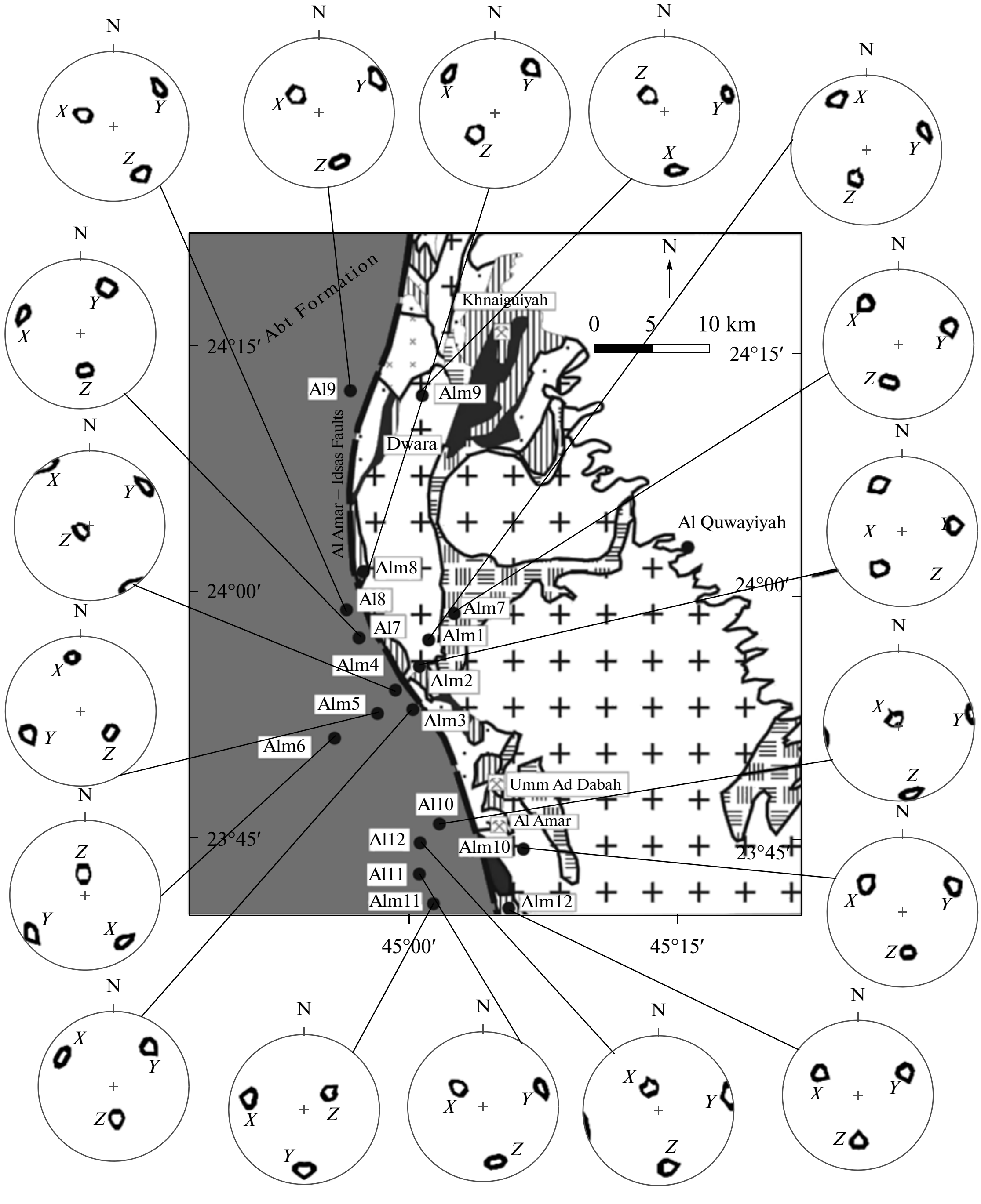

Fig. 3. Orientational data (lower hemisphere equal area projection) showing maximum extension direction (X); intermediate direction (Y) and maximum shortening direction (Z). Contours start at 3% and increment every 3% Legend see on Fig. 1.

flow-path analysis was carried out by using rotated rigid objects [45]. In samples with large equal-sized quartz, plagioclase and hornblende porphyroclasts, grains were measured for the rotation analysis. The vorticity data are shown in Figs. 5 and 6.

In the diagrams shown in Fig. 5, a distinction can be made between measurements of relatively low aspect ratio that scatter across a wide range of orientations and those with higher aspect ratio, which have a more restricted range of orientations. The critical values for Rc in investigated samples range from ~3.0 to ~6.04 (table). These values are interpreted as the critical values for Rc separating porphyroclasts that rotated freely from those which have attained a stable position during deformation. Accordingly, Wm ranges from 0.89 to 0.97 (table). The Hafafit gneisses rocks typically have feldspar porphyroclasts with aspect ratios of 1.12–4.99 in XZ sections. Low aspect ratio

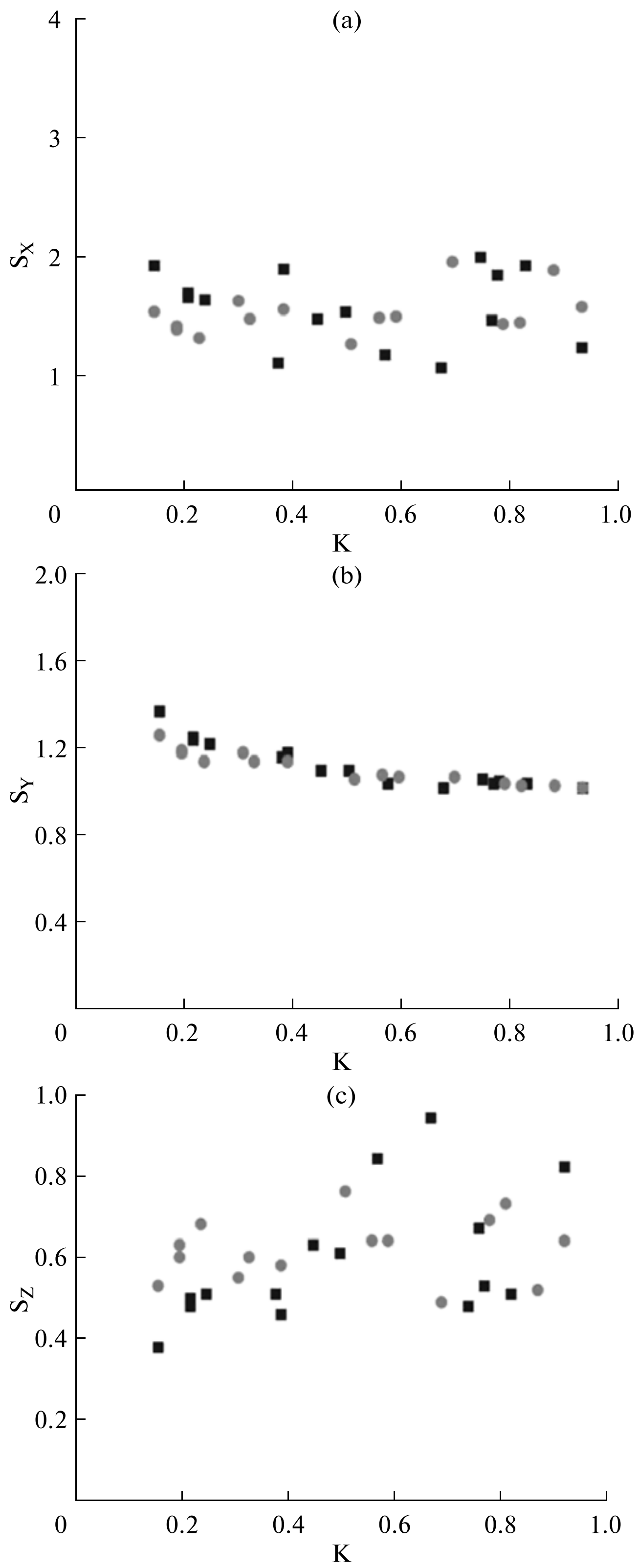

Fig. 4. Flinn diagram showing relative strain or strain symmetry as obtained by the R_f/ϕ method (Black Square) and Fry method (grey circle). a—S_X vs K showing positive correlation; b—S_Y vs K showing pronounced negative correlation; c—S_Z vs K depicting no obvious correlation.

for some samples is inclined at angles close to 45° to the mylonitic foliation and others are densely packed. With increasing aspect ratio, the angle of inclination decreases (Fig. 5). These values of aspect ratio are in harmony with flattening strains and also indicate vertical shortening normal to the main-phase foliation in the Abt Schist rocks.

In the present work, using the RGN is compared with existing methods. The ease of its use, ability for comparing natural data sets to theoretical curves, potential to standardize investigations and ability to limit ambiguity in estimating Wm, the RGN makes an important new contribution that advances the current methods for quantifying flow in shear zones. Six samples were selected for the RGN method; thee of them differ from those used in Passchier method. The values of the Wm for RGN range from 0.88 to 0.97 (Fig. 6). The Wm values obtained are same using the two methods (Figs. 5 and 6) and confirm the correctness of the flow path analysis.

DISCUSSION

Because of isochoric deformation the strain data reflect flattening strain type. The finite strain data show oblate strain symmetry in the studied mylonitized granite and metasedimentary rocks [29–31, 33, 34]. This indicates that the accumulation of ductile deformation during thrusting was not by simple shear but it involved vertical shortening produced by a component of pure shear. Pure shear-related vertical shortening caused the subhorizontal foliation in the thrusted Al Amar region. Pure and simple shear components have a non-linear relationship and make equal contributions to the overall deformation at W_m = 0.71 [36]. Using the fabric skeleton of quartz c-axis fabrics and the maximum strain ratio reveals average kinematic vorticity numbers of 0.5–0.6. These values indicate 60% pure shear component (for relationships, see [36]), which thus dominates the ductile nappe-emplacement-related deformation. O. M. K. Kassem and U. Ring [34] suggested that subhorizontal foliation by simple shear nappe stacking alone appears to be an unreasonable alternative, since it demands very high shear strains of the order of >10. Also, the rotation of elongate crystals into a subhorizontal position would lead to strain ellipses with aspect ratios of ~100 throughout the entire thickness of the nappes. Such high strains of ~100 have never been reported in the Eastern Desert of Egypt. [31] envisaged that nappe imbrication associated with a component of pure shear flattening is a general process causing flat-lying foliations. The rotation of objects by pure shear is faster than in simple shear and thus makes a pure shear component of deformation more likely for producing subhorizontal foliations across nappes. The data show oblate strain symmetry (flattening strain) in the Abt Schist Formation and metavolcanosedimentary rocks. This indicates that the time of deformation represents

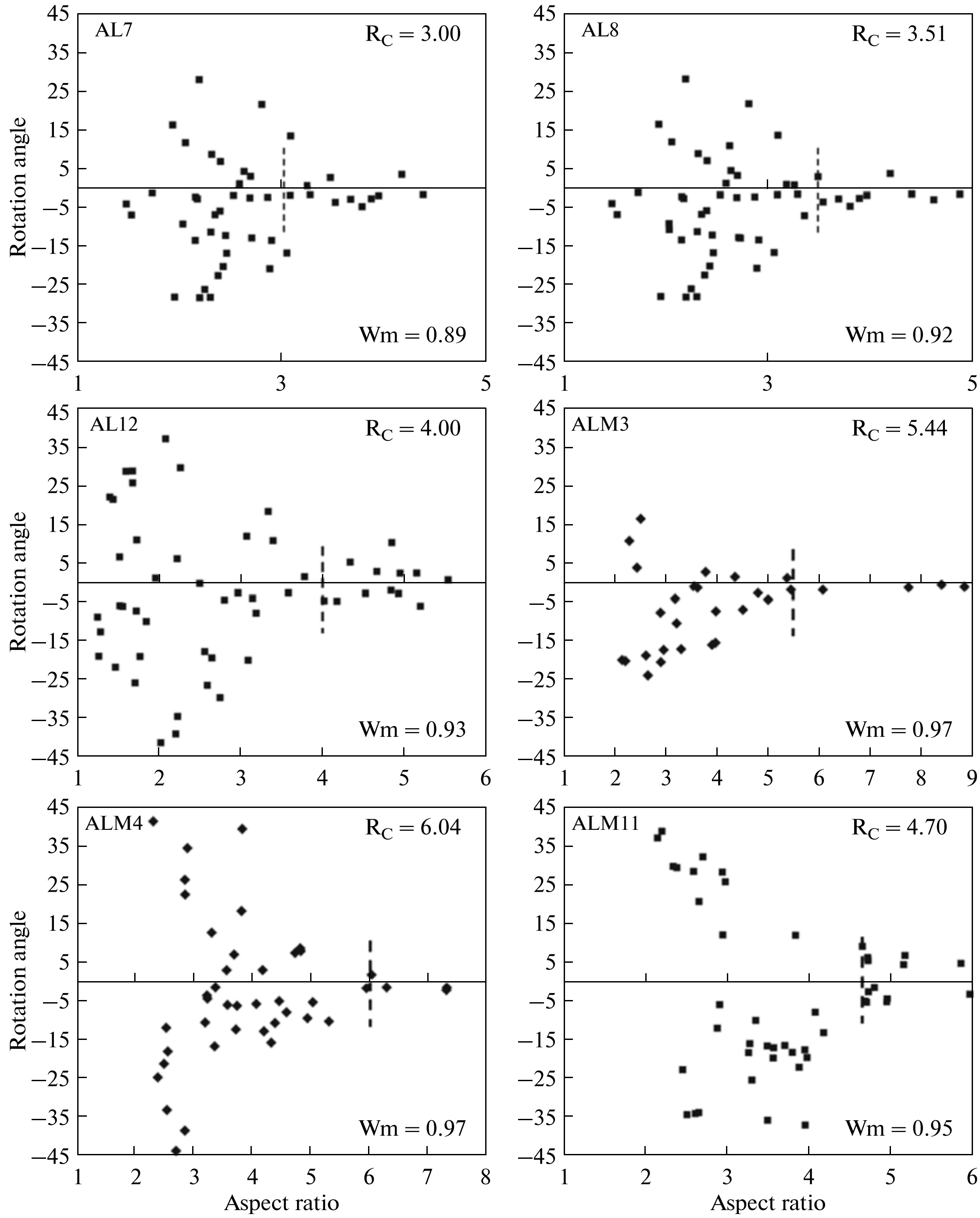

Fig. 5. Passchier's plot method; porphyroclast analyses of feldspar grains in XZ sections of gneiss; dashed line separates measurements showing wide scatter from those showing stable orientation parallel to foliation; average value of R_C for each sample is given in upper left.

the accumulation of ductile to brittle deformation during thrusting of the Abt Schist and metavolcano-sedimentary sequences of the Ad Dawadimi region over the granite and volcanic rocks of Ar Rayn region and followed by strike-slip shear. We do believe that the Al Amar fault was associated with, or followed by, flattening strain that might be a general process causing flat-lying foliations. The average kinematic vorticity numbers of the Abt Schist samples represent approximately the same values in the Al Amar area. Furthermore, finite strain in the Abt Schist Formation and metavolcano-sedimentary rocks are of the same order of magnitude as those from mylonitized granite rocks. Therefore, it is suggested that the various lithologies

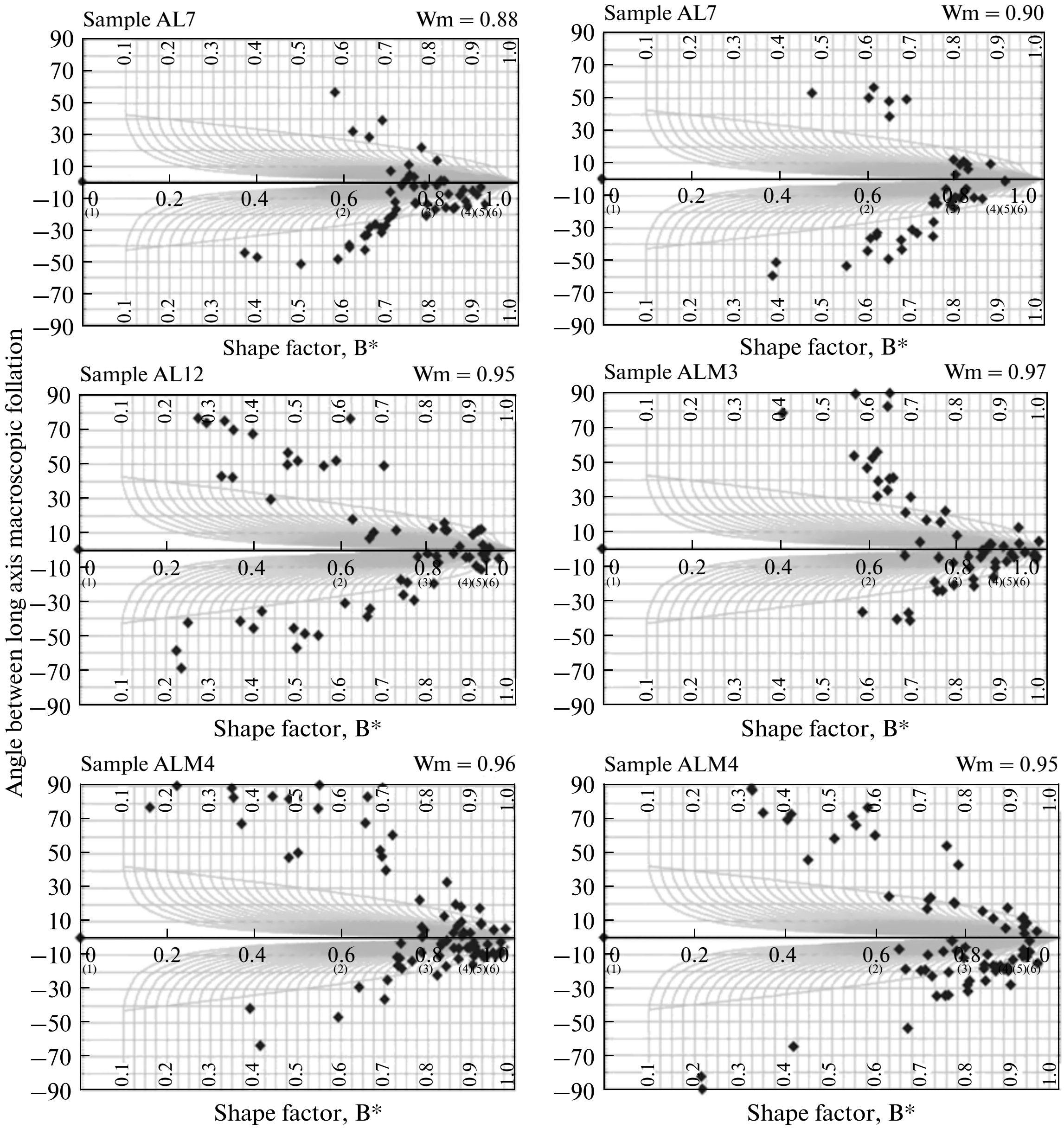

Fig. 6. The Rigid Grain Net method (RGN); porphyroclast analyses of quartz and feldspar grains.

outcropping in the study area (Abt Schist, mylonitized granite and metavolcanosedimentary rocks) are affected by the same deformation at the same time. In this case, stretching lineations during thrusting trend W/WNW and associated kinematic indicators record top to the west tectonic transport.

CONCLUSIONS

—The kinematic vorticity number obtained from the high temperature mylonitic Abt Schist in Al Amar area ranges from ~0.8 to 0.9.

—The values of the Wm for RGN range from 0.88 to 0.97.

—Results obtained from vorticity and strain analyses indicate that deformation in the area deviated from simple shear.

—The exposed lithologies in the area suffered the same deformation.

—The tectonic transport direction in the area is proposed to be towards the west.

ACKNOWLEDGMENTS

The authors would like to extend their sincere appreciation to the Deanship of Scientific Research at King Saud University for funding this research through the Research Group project no RGP-VPP-230. Special thanks are extended also to the reviewers for critical and helpful comments and for editorial handling.

REFERENCES

1. K. A. Ali, M. K. Azer, H. A. Gahlan, S. A. Wilde, M. D. Samuel, and R. J. Stern, "Age constraints on the formation and emplacement of Neoproterozoic ophiolites along the Allaqi–Heiani Suture, South Eastern Desert of Egypt," Gondwana Res. **18**, 583–595 (2010a).
2. K. A. Ali, R. J. Stern, W. I. Manton, J. I. Kimura, M. J. Whitehouse, S. K. Mukherjee, P. R. Johnson, and W. R. Griffin, "Geochemical U-Pb zircon, and Nd isotope investigations of the Neoproterozoic Ghawjah Metavolcanic rocks, Northwestern Saudi Arabia," Lithos **120**, 379–392 (2010b).
3. A. M. Al-Saleh and O. M. K. Kassem, Microstructural, strain analysis and $^{[40]}$Ar/$^{[39]}$Ar evidence for the origin of the Mizil Gneiss Dome, Eastern Arabian Shield, Saudi Arabia," J. Afr. Earth Sci. **70**, 24–35 (2012).
4. A. M. S. Al-Shanti and A. H. G. Mitchell, "Late Precambrian subduction and collision in the Al Amar–Idsas region, Kingdom of Saudi Arabia," Tectonophysics **30**, T41–T47 (1976).
5. E. H. Bailey, W. P. Irwin, and D. L. Jones, "Franciscan and related rocks, and their significance in the geology of western California," Calif. Div. Mines Bull. **183**, 177 (1964).
6. J. O. Berkland, L. A. Raymond, J. C. Kramer, E. M. Moores, and M. O'Day, "What is Franciscan?," AAPG Bull. **56**, 2295a–2302 (1972).
7. A. S. Collins and S. A. Pisarevsky, "Amalgamating eastern Gondwana: The evolution of the Circum-Indian Orogens," Earth Sci. Rev. **71**, 229 (2005).
8. D. S. Cowan, "Kinematic analysis of shears zones in sandstone and mudstone of the Shimanto belt, Shikokn, SW Japan," J. Struct. Geol. **12**, 431 (1990).
9. G. M. Cox, C. J. Lewis, A. S. Collins, G. P. Halverson, F. Jourdan, J. Foden, D. Nettle, and F. Kattan, "Ediacaran terrane accretion within the Arabian-Nubian Shield," Gondwana Res. **21**, 341 (2012).
10. I. W. D. Dalziel, "Neoproterozoic–Paleozoic geography and tectonics: review, hypothesis, environmental speculation," Geol. Soc. Am. Bull. **109**, 16–42 (1997).
11. D. Elliott, Deformation paths in structural geology," Geol. Soc. Am. Bull. **83**, 2621–2638 (1972).
12. A. Ferrand, P. Milesi, and C. Prevot, *Geologic and Metallogenic Assessment of the Al Amar Deposit*, (Deputy Ministry for Mineral Resources, Jiddah, 1985).
13. B. Freeman, "The motion of rigid ellipsoidal particles in slow flows," Tectonophysics **113**, 163–183 (1985).
14. S. K. Ghosh, and H. Ramberg, "Reorientation of inclusions by combination of pure shear and simple shear," Tectonophysics **34**, 1–70 (1976).
15. Z. Hamimi, A. El-Fakharani, and M. M. Abdeen, Polyphase deformation history and strain analyses of the post-amalgamation depositional basins in the Arabian–Nubian Shield: Evidence from Fatima, Ablah and Hammamat Basins, J. Afr. Earth Sci. **99**, 64–92 (2014).
16. Z. Hamimi, E.-S. K. El-Sawy, A. El-Fakharani, M. Matsah, A. Shujoon, and M. K. El-Shafei, Neoproterozoic structural evolution of the NE-trending Ad-Damm Shear Zone, Arabian Shield, Saudi Arabia, J. Afr. Earth Sci. **99**, 51–63 (2014).
17. Z. Hamimi, M. El-Shafei, G. Kattu, and M. Matsah, "Transpressional regime in southern Arabian Shield: Insights from Wadi Yiba area, Saudi Arabia," Mineral. Petrol. **107**, 849–860 (2013).
18. Z. Hamimi, M. Matsah, M. El-Shafei, A. El-Fakharani, A. Shujoon, M. Al-Jabali, "Wadi Fatima thin-skinned foreland FAT belt: A post amalgamation marine basin in the Arabian Shield," Open J. Geol. **2**, 271–293 (2012).
19. C. E. Hedge, *Precambrian Geochronology of Part of Northwestern Saudi Arabia, Kingdom of Saudi Arabia (Open-File Report No. 84–381)*, (U.S. Geol. Surv., Boulder, 1984).
20. J. R. Hossack, "Pebble deformation and thrusting in the Bygdin area (Southern Norway)," Tectonophysics **5**, 315 (1968).
21. G. B. Jeffery, "The motion of ellipsoidal particles immersed in a viscous fluid," Proc. R. Soc. London Ser. A **102**, 161–179 (1922).
22. G. B. Jeffrey, "The motion of ellipsoidal particles immersed in a viscous fluid," Proc. R. Soc. London Ser. A **103**, 161–179.
23. P. Johnson, "An Expanding Arabian-Nubian Shield geochronologic and Isotopic dataset: Defining limits and confirming the tectonic setting of a Neoproterozoic accretionary orogen," The Open J. Geol. **8**, 3–33 (2014).
24. P. Johnson, A. Andresen, A. S. Collins, T. R. Fowler, H. Fritz, W. Ghebreab, T. Kusky, "Late Cryogenian-Ediacaran history of the Arabian-Nubian Shield: A review of depositional, plutonic, structural, and tectonic events in the closing stages of the northern East African Orogen," J. Afr. Earth Sci. **61**, 167–232 (2011).
25. P. R. Johnson and B. Woldehaimanot, "Development of the Arabian–Nubian shield: Perspectives on accretion and deformation in the northern East African Orogen and the assembly of Gondwana," in *Proterozoic East Gondwana: Supercontinent Assembly and Breakup*, Vol. 206 of *Geol. Soc., London, Spec. Publ.* (Geol. Soc., London, 2003), pp. 290–325.
26. O. M. K. Kassem, "Determining heterogeneous deformation for granitic rocks in the Northern thrust in Wadi Mubark belt, Eastern Desert, Egypt," Geotectonics, No. (3), 244–254 (2011).
27. O. M. K. Kassem, "Kinematic Vorticity Technique for Porphyroclasts in the Metamorphic Rocks: An Example from the Northern thrust in Wadi Mubarak belt, Eastern Desert, Egypt," Arabian J. Geosci. **5**, 159–167 (2012).
28. O. M. K. Kassem, S. H. Abd El Rahim, and E. R. El Nashar, "Strain analysis and Microstructural evolution characteristic of Neoproterozoic rocks associations of Wadi El Falek, Centre Eastern Desert, Egypt," Geotectonics **46**, 379–388 (2012).
29. O. M. K. Kassem, Kinematic analysis of the Migif area in the Eastern Desert of Egypt," J. Afr. Earth Sci. **90**, 136–149 (2014).
30. O. M. K. Kassem and Z. Hamimi, "Application of finite strain technique for deformed lithologies in Al Amar suture, Eastern Arabian Shield," The Open Geol. J. **8**, 97–106 (2014).
31. O. M. K. Kassem and U. Ring, Underplating-related finite-strain patterns in the Gran Paradiso massif, Western Alps, Italy: heterogeneous ductile strain superimposed on a nappe stack," J. Geol. Soc. London, U. K.) **161**, 875–884 (2004).

32. A. Kröner, P. Linnebacher, R. J. Stern, T. Reischmann, W. Manton, I. M. Hussein, Evolution of Pan-African island arc assemblages in the southern Red Sea Hills, Sudan, and in southwestern Arabia as exemplified by geochemistry and geochronology," Precambrian Res. **53**, 99–118 (1991).
33. R. D. Law, M. P. Searle, and R. L. Simpson, "Strain, deformation temperatures and velocity of flow at the top of the Greater Himalayan Slab, Everest Massif, Tibet," J. Geol. Soc. London, U. K.) **161**, 305–320 (2004).
34. G. S. Lister and P. F. Williams, "The partitioning of deformation in flowing rock masses," Tectonophysics **92**, 1–33 (1983).
35. L. E. Malvern, *Introduction to the Mechanics of a Continuous Medium* (Prentice-Hall, Englewood Cliffs, NJ, 1969).
36. W. D. Means, B. E. Hobbs, G. S. Lister, and P. F. Williams, "Vorticity and non-coaxiality in progressive deformations," J. Struct. Geol. **2**, 371–378 (1980).
37. J. G. Meert and T. H. Torsvik, "The making and unmaking of a supercontinent: Rodinia revisited," Tectonophysics **375**, 261–288 (2003).
38. R. D. Nance, J. B. Murphy, and M. Santosh, "The supercontinent cycle: A retrospective essay," Gondwana Res. **25**, 4–29 (2014).
39. C. W. Passchier, "Flow in natural shear zones-the consequences of spinning flow regimes," Earth Planet. Sci. Lett. **77**, 70–80 (1986).
40. C. W. Passchier, "Stable positions of rigid objects in non-coaxial flow-a study in vorticity analysis," J. Struct. Geol. **9**, 679–690 (1987).
41. C. W. Passchier, "Reconstruction of deformation and flow parameters from deformed vein sets," Tectonophysics **180**, 185–199 (1990).
42. C. W. Passchier and R. A. Trouw, *Microtectonics* (Springer, Berlin, 1995).
43. C. W. Passchier and J. L. Urai, "Vorticity and strain analysis using Mohr diagrams," J. Struct. Geol. **10**, 755–763 (1988).
44. J. G. Ramsay, *Folding and Fracturing of Rocks* (McGraw Hill, London, 1967).
45. J. G. Ramsay and M. I. Huber, *The Techniques of Modern Structural Geology*, Vol. 1: *Strain Analysis* (Academic press, New York, 1983).
46. U. Ring, "Exhumation of blue schists from Samos Island," Geol. Soc. Greece Bull. **32**, 97–104 (1998).
47. U. Ring and M. T. Brandon, "Deformation and mass loss in the Franciscan subduction complex: Implications for exhumation processes in accretionary wedges," in *Exhumation processes: Normal Faulting, Ductile Flow, and Erosion*, Vol. 154 of *Geol. Soc. London Spec. Publ.*, Ed. by U. Ring, M. T. Brandon,, G. S. Lister, and S. D. Willett (London, 1999), pp. 55–86.
48. U. Ring, M. T. Brandon, and A. Ramthun, "Solution-mass-transfer deformation adjacent to the Glarus thrust, with implications for the tectonic evolution of the Alpine wedge in eastern Switzerland," J. Struct. Geol. **23**, 1491 (2001).
49. U. Ring and O. M. K. Kassem, "The nappe rule: Why does it work?," J. Geol. Soc. London, U. K.) **164**, 1109–1112 (2007).
50. C. Simpson and D. G. De Poar, "Strain and kinematic analysis in general shear zones," J. Struct. Geol. **15**, 1–20 (1993).
51. C. Simpson and D. G. De Paor, "Practical analysis of general shear zones using the porphyroclast hyperbolic distribution method: An example from the Scandinavian Caledonides," in *Evolution of Geological Structures in Micro- to Macro- Scales*, Ed. by S. Sengupta (Chapman & Hall, London, 1997), pp. 169–184.
52. C. Simpson and S. M. Schmid, "An evolution of criteria to determine the sense of movement of sheared rocks," Geol. Soc. Am. Bull. **94**, 1281–1288 (1983).
53. R. J. Stern, "Arc assembly and continental collision in the Neoproterozoic East African Orogen: Implications for the consolidation of Gondwanaland," Ann. Rev. Earth Planet. Sci. **22**, 315–319 (1994).
54. R. J. Stern and P. R. Johnson, "Continental lithosphere of the Arabian Plate: A geologic, petrologic, and geophysical synthesis," Earth-Sci. Rev. **101**, 29–67 (2010).
55. 55.Stoeser, D.B., Stacey, J.S., "Evolution, U–Pb geochronology and isotope geology of the Pan-African Nabitah orogenic belt of the Saudi Arabian Shield," in *The Pan-African belt of NE African and Adjacent Areas*, Ed. by S. El-Gaby and R. O. Greiling, (Friedrich, Viewig and Sohn, Braunschweig, 1988), pp. 227–288.
56. B. Tikoff and C. Teyssier, "Strain and fabric analyses based on porphyroclast interaction," J. Struct. Geol. **16**, 477–491 (1994).
57. S. R. Wallis, "Vorticity analysis in a metachert from the San-bagawa Belt, SW Japan," J. Struct. Geol. **14**, 271–280 (1992).
58. S. R. Wallis, "Vorticity analysis and recognition of ductile extension in the Sanbagawa belt, SW Japan," J. Struct. Geol. **17**, 1077–1093 (1995).
59. T. R. Worsley, R. D. Nance, and J. B. Moody, "Global tectonics and eustasy for the past 2 billion years," Mar. Geol. **58**, 373–400 (1984).
60. T. R. Worsley, R. D. Nance, and J. B. Moody, "Proterozoic to recent tectonic tuning of biogeochemical cycles," in *The Carbon Cycle and Atmospheric CO_2: Natural Variations Archean to Present*, Vol. 32 of *Geophysical Monograph*, Ed. by E. T. Sunquist and W. S. Broecker (Am. Geophys. Union, 1985), pp. 561–572.
61. T. R. Worsley, R. D. Nance, and J. B. Moody, "Tectonic cycles and the history of the Earth's biogeochemical and paleoceanographic record," Paleoceanography **1**, 233–263 (1986).
62. Z. A. H. Nawab, "Evolution of the Al Amar Idasas region of the northern part of the Arabian Shield (Kingdom of Saudi Arabia)," Bull. Bur. Rech. Geol. Min., Sect. 2: Geol. Appl. (Fr.), Nos. 1–2, 1–19 (1978).
63. Borghi, A., Compagnoni, R. & Sandrone, R., Evoluzione "Tettonica Alpina Del settore setten trionale Del Massiccio Del Gran Paradiso (Alpi Occidentali)," Atti Ticinensi di Scienze Della Terra **1**, 137–152 (pp.).
64. A. Borghi, R. Compagnoni, and R. Sandrone, "Composite P–T paths in the Internal Penninic Massifs of the Western Alps: Petrological constraints to their thermo-mechanical evolution," Eclogae Geol. Helv. **89**, 345–367 (1996).
65. O. M. K. Kassem and S. Abdel Raheim, "Finite strain analysis for the Metavolcanic sedimentary rocks in the Gabel El Mayet region, Central Eastern Desert, Egypt, J. Afr. Earth Sci. **58**, 321–330 (2010).
66. S. Mordechai, "Tracing the plume material in the Arabian-Nubian Shield," Precambrian Res. **123**, 223–234 (2003).

SPELL: OK